EFFECT OF HYDROTHERMAL TEMPERATURE ON STRUCTURAL, MORPHOLOGICAL AND OPTICAL PROPERTIES OF FACILE HYDROTHERMALLY SYNTHESISED Cu_2ZnSnS_4 NANOMATERIALS

[1]Mohammed,K. I.,[2]Mohammed, I. K., [2]Ibrahim,S. O.,[2]Abubakar, A. A., [3]Yabagi, J. A.,[2]Isah, K. U.,[2]Uno, E. U., [4]Abdullah, M.,[5]Nayan, N. and [5]Khairul, M. A.

[1]*Department of Physics, School of Sciences, Niger State Polytechnic, Zungeru, Niger State, Nigeria*

[2]*Department of Physics, School of Physical Sciences, Federal University of Technology, Minna, Niger State, Nigeria*

[3] *Department of Physics, Faculty of Sciences, Ibrahim Badamasi Babangida University, Lapai, Niger State, Nigeria*

[4]*Department of Chemistry, School of Physical Sciences, Federal University of Technology, Minna, Niger State, Nigeria*

[5]*MiNT-SRC, Institute for Integrated Engineering (I^2E), Universiti Tun Hussein, Onn, Malaysia*

*Corresponding author email: kimpa@futminna.edu.ng

ABSTRACT

Cu_2ZnSnS_4 (CZTS), semiconductor has proven to be a low cost promising absorber material with high optical absorption coefficient and an ideal band gap for photovoltaic applications. This work presents a facile hydrothermal synthesis of a CZTS nanocrystalline material using Polyacrylic acid (PAA) as surfactant. The effect of hydrothermal synthesis temperatures between 150 and 270^{o}C (in steps of 40^{o}C) on the phase, composition, microstructure and morphology were investigated. Pure kesterite CZTS were obtained, composed of spherical shaped flower-like aggregated nanoparticles, with particle sizes ranging between 10 and 19 nm. The Cu/Zn/Sn ratio were near the ideal stoichiometric ratio for samples synthesised at 150 and 170^{o}C, while those synthesized at 230 and 270 hydrothermal temperatures show considerable deviation. The obtained bandgaps were about 1.51 eV.

Keywords: semiconductor, hydrothermal, synthesis.

INTRODUCTION

Cu_2ZnSnS_4 (CZTS) is a quaternary chalcogenide, which is an emerging solar cell material derived from the CIGS structure by the isoelectronic substitution of expensive and toxic *In* and *Ga* atoms by benign, earth-abundant and low cost elements one Zn and one Sn atom. It has near-optimum direct band gap energy of 1.5 eV and a large absorption coefficient (>104 cm-1) and thus its extensive application as absorber material in thin film solar cell (Choubrac*et al*., 2012). Thin film absorber layers of CZTS can be made from the slurry of its nanocrystals through cost-effective easily scalable techniques such as spin coating, doctor blading and screen printing.

Aside from its application as absorber materials in thin film solar cell, the low resistivity of Pt in liquid electrolyte and its high cost has necessitated the need for its replacement as counter electrode (CEs) in Dye sensitised solar cell by metal based sulphides such as CZTS. CZTS has been shown to exhibit performance as CE that is competitive with Pt (Roy *et al*., 2018). Minority carrier collection in CZTS thin films are favorable enhanced by grain boundaries, moreover its crystal structure also allows for some deviation in its stoichiometry, thus making its deposition easier (Choubrac*et al*., 2012 & Li *et al*., 2012). Various deposition and synthesis techniques such as pulsed laser deposition, thermal evaporation, and sputtering techniques have been employed for the synthesis of CZTS (Chan *et al*., 2010; Tanaka *et al*., 2006 & Shin *et al*., 2011), they are vacuum based and have the disadvantage of the use of complicated equipment, high production costs.

In this work facile low cost hydrothermal synthesis has been employed in the synthesize CZTS nanocrystalline material at hydrothermal temperatures of 150, 190, 239 and 270 °C. The CZTS nanoparticles were characterized for phase composition, morphology, microstructure and optical absorption using Raman spectrometry, x-ray diffraction (XRD), scanning electron microscope (SEM) and UV–vis spectrophotometer.

METHODS

Experimentals

The CZTS nanoparticles were synthesised using Copper (II) chloride dihydrate ($CuCl_2.2H_2O$, 99.9 % Sigma Aldrich), Zinc chloride ($ZnCl_2$, 99.9m% BDH), Tin (IV) chloride pentahydrate ($SnCl_4.5H_2O$, 99.8 %, Fluker), Thioacetamide (C_2H_5NS, 98.9 %, Merck) as source of

Sulfur and Polyacrylic acid (PAA, 99.0 %, Fisher) as the surfactant.

To synthesise the nanoparticles, 0.2 mmol of $CuCl_2.2H_2O$, 0.1 mmol of $ZnCl_2$, 0.1 mmol of $SnCl_4.5H_2O$, 0.5 mmol of C_2H_5NS and 1.0 g of PAA were dissolved in 36 ml of deionised water under magnetic stirring. The resulting solution was transferred to a Teflon-lined stainless steel autoclave of 45 ml capacity, which was then sealed and maintained at 150 °C, 190 °C, 230 °C and 270 °C each for 24 h, and the autoclave in each case was allowed to cool to room temperature naturally. The samples were labelled 150-_24, 190_24, 230_24 and 270_24 for reaction temperature of 150, 190, 239 and 270 °C respectively. The black precipitate that resulted from the autoclaving of each sample was centrifuged and washed with deionised water, absolute ethanol and acetone for several times. Finally, the products were vacuum-dried at 80 °C for 5 h. The resulting nanoparticles were deposited as thin film on FTO coated soda lime glass (FTO/SLG) substrate and annealed in a graphite box containing sulphur powder at 550 °C for 30 min in a rapid thermal annealing processing (RTP) system with a heating rate of 10 °C/min. A static annealing atmosphere of 0.3 atm argon was supplied in the RTP furnace.

Characterisations

The phase and crystallographic structure of the samples were identified by X-ray diffraction (XRD, PANanalyticalXPert Pro Multi-Purpose Diffractometer (MPD), CuKα, λ = 0.154056 nm). The Raman spectra of the samples were recorded with a Raman spectrometer (Xplora Plus, Horiba Scientific Raman microscope) with a 785 nm excitation laser to distinguish possible secondary phases in the films. The morphology and quantitative elemental analysis of the samples were characterised by scanning electron microscopy (SEM, JEOL 7600F) at an acceleration voltage of 20.0 kV combined with an energy dispersive X-ray spectroscopy (EDS). Ultraviolet-visible (UV-vis) absorption spectrum of the samples was measured at room temperature using a Shimadzu UV-1800 spectrophotometer.

RESULTS AND DISCUSSIONS

XRD Analysis

Figure 1 show the XRD patterns of the CZTS thin film samples obtained at different temperatures.

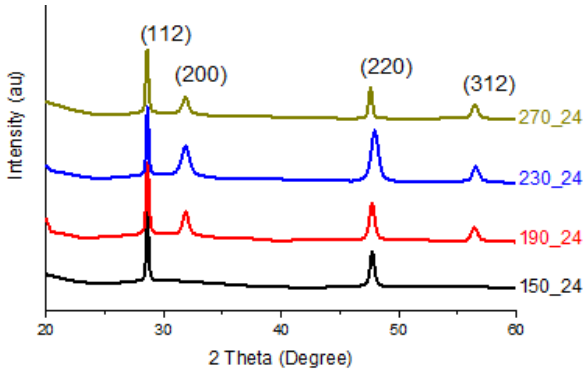

Figure 1: XRD patterns for reaction temperature variation of CZTS thin films

From the XRD pattern, all films show preferential orientation along (112) plane having the most prominent peak. The peaks at 2θ values of 28.59°, 47.70°, 33.04 and 57.54 correspond to lattice planes (112), (220), (200) and (312) respectively are indexed to the corresponding crystal planes kesterite CZTS (JCPDS 01-75-4122) with cell parameters a = b = 0.5427 nm and c = 1.0848 nm (Schafer and Nitsche, 1974 &Zheng*et al.*, 2019). At 150 °C, only (112) and (220) peaks were observed but at higher hydrothermal temperature of 190, 230 and 270 °C, the peaks (200) and (312) were observed in addition to the (112) and (220) this is also in agreement with literature reports [9]. The peak of CZTS at 2θ value of 28.59° is observed to shift left by 0.26 degrees in 190_24 sample. This shift might be due to changes in d_{112}-spacing values of 2.947 Å of the sample Tiong*et al.*, 2014). The other samples had d_{112}-spacing in close agreement with theoretical values (CZTS: JCPDS 26-0575) as shown in Table 1.

Table 1: Lattice parameter and crystallite sizes D of samples

Sample ID	a (Å)	c (Å)	d_{111}-spacing (Å)	D (nm)
150_24	5.43	10.86	3.122	19
190_24	3.82	19.97	2.947	10
230_24	5.41	10.75	3.125	15
270_24	5.41	10.75	3.126	16
Theoretical value (CZTS:JCPDS 26-0575)	5.427	10.848	3.126	-

The crystallite size D were determined from the most prominent (112) Debye Scherer's formula [10]in equation (1):

$$D = \frac{k\lambda}{\beta Cos\theta} = \frac{0.9\lambda}{\beta Cos\theta} \quad (1)$$

Where β = full width at half maximum (FWHM), θ = diffraction angle k = Shape factor and λ = wavelength. The values obtained were 19, 10, 15 and 16 nm for values of FWHM the 150_24, 190_24, 230_24 and 270-_24 samples respectively.

Raman Spectroscopy Analysis

Definitive structural analysis and electronic excitation states of the lattice that provide information on possible secondary phases in a material is provided by Raman Spectroscopy. Raman scattering gives a more definitive structure analysis (Das *et al*., 2018). The Raman spectra shown in Figure 2, clearly reveal the peaks 338 cm^{-1}, 351 cm^{-1} and 252 cm^{-1} which are CZTS peaks for samples 150_24, 190_24 and 230_24 (Fernandes*et al*., 2009). At temperatures higher than 150 ^{o}C the 275cm^{-1} peak appearedusually associated with ZnS (Nagoya *et al*., 2010).

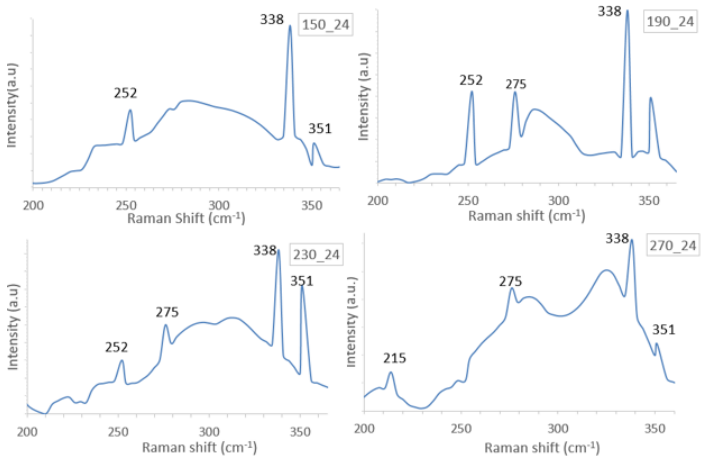

Figure 2: Raman spectra for CZTS thin film samples synthesised at different reaction temperatures

At the temperature of 270 ^{o}C, the 215 cm^{-1} peak was observed. The 215 cm^{-1} peak is SnS_2 secondary phase (Price *et al*., 1999). For CZTS obtained at 150^{o}C only the 252 cm^{-1}, 338 cm^{-1} and 351 cm^{-1} peaks were observed which are all pure phase peaks of CZTS.

SEM/EDS Analysis

Figure 3 show the SEM image of the CZTS thin film samples obtained at different temperatures. The SEM images illustrates that the thin films were composed mainly a gradual progression from flower-like quasi-sphere to spherical aggregations composed of agglomerated nanosheets and nanopetals.

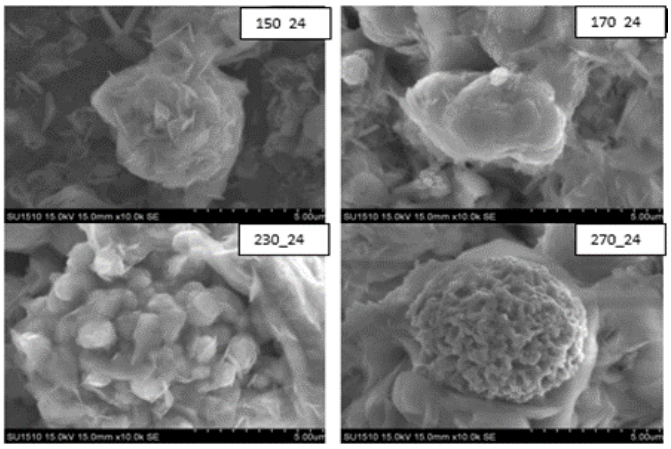

Figure 3: SEM images for the CZTS thin film samples synthesised different reaction temperatures

The elemental composition of the samples is shown in Table 2. The ideal CZTS stoichiometric compositional entails Cu/(Zn + Sn) and (Zn/Sn) be equals 1, while the ideal Cu:Zn:Sn:S stoichiometric value is 2:1:1:4. The 150_24 and 190_24 samples reveal near ideal compositional ratio for Cu/(Zn + Sn) of 0.91 and 0.84, Zn/Sn ratio of 0.87 and 0.74 respectively, these values though shows they are both Cu poor and Zn poor as seen in table 1. Cu/(Zn + Sn) atomic ratio of near 0.85 have however been reported to show good optoelectronic properties and best device efficiency (Katagiri*et al.*, 2008).

Table 2: Lattice parameter and crystallite sizes D of samples

	Atomic percentage				Ratio			
Sample	Cu (at.%)	Zn (at.%)	Sn (at.%)	S (at.%)	Cu/(Zn+Sn)	Zn/Sn	Cu:Zn:Sn:S	Grain size (nm)
Ideal	25.0	12.5	12.5	50.0	1.00	1.00	2.00:1.00:1.00:4.00	-
150_24	23.1	11.8	13.5	48.9	0.91	0.87	1.96:1.00:1.14:4.14	17
190_24	22.5	11.4	15.4	47.5	0.84	0.74	1.97:1.00:1.35:4.17	11
230_24	22.4	7.4	19.5	47.9	0.83	0.38	3.03:1.00:2.14:6.47	13
270_24	23.4	7.1	17.8	48.7	0.94	0.40	3.30:1.00:2.51:6.86	12

Evidently increasing hydrothermal temperature leads to decreasing Zn/Sn atomic ratio and shows the samples are Sn rich and Zn poor, with 230_24 and 290_24 showing significantly high Sn content compared to Zn. The slight Sn rich and Zn poor composition for 150_24 and 190_24 and the significant Sn rich and Zn poor composition at 230_24 and 290_24 may be ascribed to the lower reactivity of Zn^{2+} ions precursor than Sn^{4+} ions precursor making the reagents to contain more Zn salt than the stoichiometric amount for the expected cation ratios (Chalapathi*et al.*, 2015). The Cu:Zn:Sn:S ratios of 1.96:1.00:1.14:4.14 and 1.97:1.00:1.35:4.17 for the 150_24 and 190_24 samples respectively were close to ideal stoichiometric value of 2:1:1:4. Samples 230_24 and 290_24 however show significant deviation from ideal CZTS composition exhibiting very high Cu and S content. Thus higher hydrothermal temperature tends to favour higher Cu and S content.

Optical Absorption Analysis

Figure 4 show the spectral transmittance curve of the films obtained from the UV-vis spectrophotometer measurements for the wavelength range of 350-1000 nm.

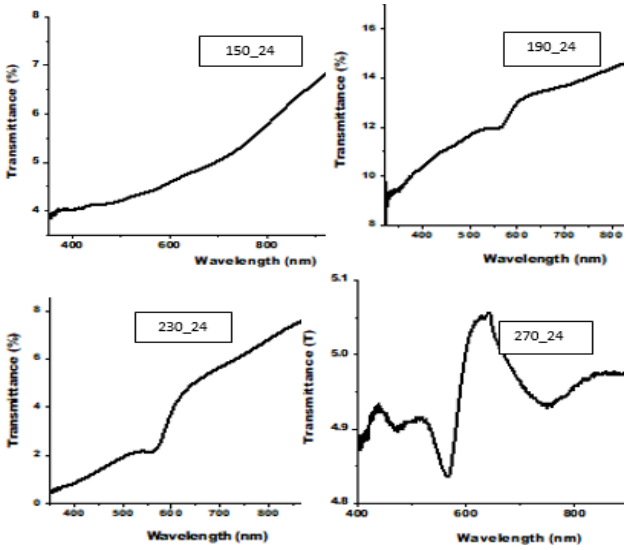

Figure 4: Optical transmittance curves

The transmittance curves show the samples have very strong absorption in the visible region. From the transmittance spectra the optical absorption coefficient of the CZTS films were estimated using the relation in equation (2):

$$\alpha = \frac{1}{d}\ln\frac{1}{T} \quad (2)$$

Where d is film thickness and T is the transmittance.

For a direct band gap material, the absorption coefficient satisfies the relation in equation (3):

$$(\alpha h\nu)^2 = A(h\nu - E_g) \quad (3)$$

whereα, ν, E_g and A are the absorption coefficient, light frequency, band gap energy and a constant respectively. The direct band gap E_g calculated by extrapolating the linear portion of the curves of $(\alpha h\nu)^2$ vs. $(h\nu)$ which gives the values of E_g as follows; 1.51 eV for sample 150_24, 1.52 eV for sample 190_24, 1.52 eV for sample 230_24 and 1.50 eV for sample 270_24 respectively (Figure 5), which are in good agreement with the reported value in literature (Chalapathi*et al*., 2015).

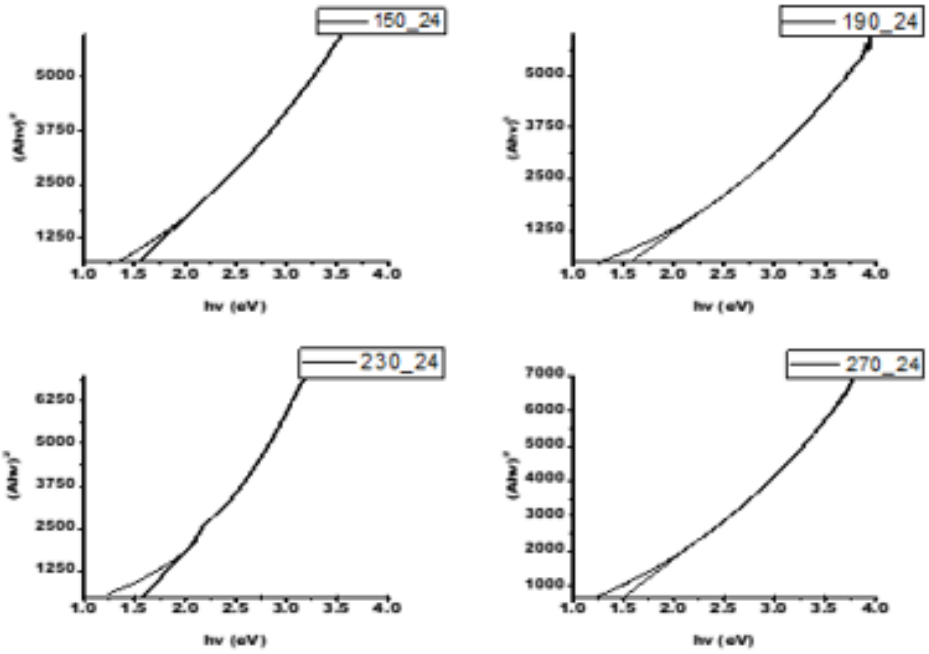

Figure 5: $(\alpha h\nu)^2$ vs. $(h\nu)$ plots of the samples

This value for a direct band gap material is ideal for application as absorber layer and counter electrode of solar energy devices.

CONCLUSION

Nanocrystalline CZTS were synthesised using hydrothermal method while varying the hydrothermal synthesis temperature. Influence of the synthesis temperature on structural, morphology and optical properties of CZTS films were investigated by x-ray diffraction (XRD), Raman spectroscopy, scanning electron microscopy (SEM), UV-Visible spectroscopy. we found that the reaction temperature plays a vital role for the crystal phase and morphology control. Kesterite CZTS composed of flower-like quasi-sphere and spherical aggregations of agglomerated nanosheets and nanopetals with preferred (112) orientation were obtained. Lower hydrothermal temperatures of 150 °C and 190 °C exhibited a near stoichiometric Cu:Zn:Sn:S ratios of 1.96:1.00:1.14:4.14 and 1.97:1.00:1.35:4.17. Samples 230_24 and 290_24 however show significant deviation from ideal CZTS composition exhibiting very high Cu and S content. Thus higher hydrothermal temperature tends to favour higher Cu and S content. Also higher hydrothermal temperature leads to decreasing Zn/Sn atomic ratio and shows the samples are Sn rich and Zn poor, with hydrothermal temperatures of 230 °C and 290 °C showing significantly high Sn content compared to Zn. All the sample exhibited optical band gaps close to 1.5 eV.

ACKNOWLEDGEMENT

We wish to acknowledge the Microelectronics and Nanotechnology Shamsuddin Research Centre (MiNT-

SRC), Institute for Integrated Engineering (I^2E), Universiti Tun Hussein Onn Malaysia for all the characterisations.

REFERENCES

Chalapathi, U., Uthanna, S. & Raja, S. (2015). Growth of Cu2ZnSnS4 thin films by a two stage Process-Effect of incorporating of sulfur at the precursor stage. *Sol. Ener. Mat. Sol*. Cells, (132), 476-484.

Chan, C.P., Lam, H., & Surya, C. (2010). "Preparation of Cu2ZnSnS4 films by electrodeposition using ionic liquid. *Sol Ener. Mater Sol Cells*, 94(2), 207–211.

Choubrac, L., Lafond, A., Guillot-Deudon, C., & Moëlo and S. Jobic, Y. (2012). Structure flexibility of the Cu2ZnSnS4 absorber in low-cost photovoltaic cells: from the stoichiometric to the copper-poor compounds" *Inorg Chem*, l(51), 3346-3348.

Das, S., Sa, K., Mahakul, P. C., Raiguru, J., Alam, I., Subramanyam, B. & Mahanandia, P. (2018). Synthesis of quaternary chalcogenide CZTS nanoparticles by a hydrothermal route. *Material Science and Engineering*, 338, 3-6.

Fernandes, M., Cao, L., Zhang, B. L. & Jiang, J. C. (2009).One step deposition of CZTS thin films for solar cells. *Sol. Ener. Mat. Sol. Cells*, 117, 81-86.

Ge, J., Jiang, J., Yang, P. X., Peng, C., Huang, Z., Zuo, S., Yang, L. & Chuab, J. (1998). A 5.5% efficient co-electrodeposited ZnO/CdS/Cu2ZnSnZ4/Mo thin film solar cell. *Sol. Ener. Mat. Sol. Cells*, 125, 20-26.

Katagiri, H., Jimbo, K., Yamada, S., Kamimura, T., Maw, W. S., Fukano, T., Ito, T. & Motohiro, T. (2008). Enhanced conversion efficiencies of CZTS-based thin film solar cells by using preferential etching technique. *Applied Physics Express*, (4), 412-415.

Li, J. B., Chawla, V. & Clemens, B. M. (2012).Investigating the Role of Grain Boundaries in CZTS and CZTSSe Thin Film Solar Cells with Scanning Probe Microscopy. *Adv Mater*, 24, 720-723.

Nagoya, K. V., Pawara, S. M., Shinb, S, W., Moona, J. H. & Kima, P. S. (2010). Electrosynthesis of CZTS films by sulfurization of CZT precursor: effect of soft annealing treatment. *Appl. Surf. Sci*., 238, 74-80.

Price, D. B., Mitzi, O., Gunawan, T. K. & Wang, K. (1999). The path towards a high performance solution-processed kesterite CZTS. *Sol. Ener. Mat. Sol. Cells*, 95, 1421-1436.

Roy, A., Sujatha Devi, P., Karazhanov, S., Mamedov, D., Kumar Mallick, T. & Sundaram, S. (2018). A Review on Applications of Cu2ZnSnS4 as Alternative Counter Electrodes in Dye-Sensitized Solar Cells.*AIP Advances*, 8, 701-707.

Schäfer, W. & Nitsche, R. (1974). Tetrahedral quaternary chalcogenides of the type Cu2–II–IV–S4 (Se4). *Mater. Res. Bull*, 9, 645–654.

Shin, S. W., Pawar, S.M., Park, C. Y., Yun, J. H., Moon, J., Kim J. H. & Lee, J. Y. (2011). Studies on Cu2ZnSnS4 (CZTS) absorber layer using different stacking orders in precursor thin films. *Sol Energy Mater Sol Cells*, 95(12) 3202–3206.

Tanaka, T., Kawasaki, D., Nishio, M., Guo, Q. & Ogawa, H. (2006).Fabrication of Cu2ZnSnS4 thin films by co-evaporation. *Phys Status Solidi C*, 3(8) 2844–2847.

Tiong, V. T., Hreid, T., Will, G., Bell, J. & Wang, H. (2014). Polyacrylic acid assisted synthesis of CU2ZnSnS4 by hydrothermal method. *Science of Advanced Materials*, 6(7), 1467-1474.

Zheng, X., Liu, Y., Zhang, N., Hou, J., Zhao, G. & Fang, Y. (2019). Fabrication of Cu2ZnSn(S,Se)4 thin film solar cell devices based on printable nano-ink. *Bull. Mater. Sci*., 1(42), 68.